Solution Assembly of Organized Carbon Nanotube Networks for Thin-Film Transistors

Melburne C. LeMieux,[†] Seihout Sok,[†] Mark E. Roberts,[†] Justin P. Opatkiewicz,[†] Derrick Liu,[†] Soumendra N. Barman,[†] Nishant Patil,[‡] Subhasish Mitra,[‡] and Zhenan Bao[†,*]

[†]Department of Chemical Engineering, Stanford University, Stauffer III, 381 North-South Mall, Stanford, California 94305-5025, and [‡]Department of Electrical Engineering, Stanford University, David Packard Building, 350 Serra Mall, Stanford, California 94305-5025

ABSTRACT Ultrathin, transparent electronic materials consisting of solution-assembled nanomaterials that are directly integrated as thin-film transistors or conductive sheets may enable many new device structures. Applications ranging from disposable autonomous sensors to flexible, large-area displays and solar cells can dramatically expand the electronics market. With a practical, reliable method for controlling their electronic properties through solution assembly, submonolayer films of aligned single-walled carbon nanotubes (SWNTs) may provide a promising alternative for large-area, flexible electronics. Here, we report SWNT network TFTs (SWNTntTFTs) deposited from solution with controllable topology, on/off ratios averaging greater than 10^5, and an apparent mobility averaging 2 $cm^2/V \cdot s$, without any pre- or postprocessing steps. We employ a spin-assembly technique that results in chirality enrichment along with tunable alignment and density of the SWNTs by balancing the hydrodynamic force (spin rate) with the surface interaction force controlled by a chemically functionalized interface. This directed nanoscale assembly results in enriched semiconducting nanotubes yielding excellent TFT characteristics, which is corroborated with μ-Raman spectroscopy. Importantly, insight into the electronic properties of these SWNT networks as a function of topology is obtained.

KEYWORDS: aligned nanotube network · thin-film transistor · directed assembly

Ultrathin films of single-walled carbon nanotubes (SWNTs) represent a unique class of materials particularly interesting and potentially beneficial for a diverse range of applications including high-strength hybrid nanocomposites,[1] growth platforms for neuronal circuits,[2] highly sensitive chemical/biological sensors,[3−6] electrode materials for solar cells,[7,8] and as active elements in electronic devices.[9,10] Applied SWNT research and development efforts divested across many fields are a result of their superior electronic and mechanical properties, yet the potential remains to be realized for any widespread application. This is partly due to limitations in reproducible directed assembly that also hinders the understanding of their fundamental properties, as well as chirality purification. The desired layout, or topology, of the SWNT network (SWNTnt) will depend on the application and, therefore, may have a wide variance of density, alignment, and bundling. For example, SWNT-based sensors should have debundled, nonburied semiconducting tubes with minimal percolation paths for unambiguous response,[5,11] while electrode materials require higher density and an optimal degree of bundling of perhaps metallic tubes[12] to maximize current carrying capacity.[7,13] For transparent electrode applications, the alignment can also play a crucial role as the degree of anisotropy can impact the optoelectrical properties.[14]

The ability to tune SWNTnt topology is especially important for SWNTnt-based thin-film transistors (SWNTntTFTs). Although single-tube TFT devices can potentially achieve the intrinsic mobility of a semiconducting SWNT,[15] single-tube assembly method is extremely challenging to scale up, and not technologically practical for large-area applications. Thin films of SWNTs, from random to well-aligned networks, represent a promising path to scalable device manufacturing.[16−18] The ability to tune the topology of these networks represents an important challenging issue in nanotechnology and is central to the performance and charge transport in such devices. Experimental and theoretical studies of SWNTntTFTs have shown that the degree of alignment and density of the SWNTs dramatically influences charge transport.[19,20] Another significant issue is high contact resistance at tube junctions. While having a higher density of tubes can increase the source−drain current (I_{DS}) by creating more percolation paths, the increased density also leads to an increase in the probability of having a percolation path dominated by metallic species and, therefore, shorted TFTs. Here, we show high alignment can increase density without significantly raising junction points; however, a certain level of misalignment is required for percolation, and it is well-known that density and alignment directly influence the SWNTntTFT behavior.[20] Moreover, the level of contact resistance at intertube junctions depends on overlap angle such that an optimal atomic registry exists at this molecular junc-

*Address correspondence to zbao@stanford.edu.

Received for review July 19, 2009 and accepted November 13, 2009.

Published online November 19, 2009.
10.1021/nn900827v

tion,[21] as well as chirality where the resistance is much lower at all-semiconducting (SC) junctions than metal (MET)−SC junctions.[22]

The challenges associated with network assembly/alignment is preceded by another persistent problem unique and fundamental to nanotubes: all synthesis methods produce nanotubes with both semiconducting and metallic chiralities.[23] As a result, typical SWNTntTFTs have an on/off ratio that is typically quite poor, 100 or lower in as-deposited transistors[24] without "burnoff" metallic tubes.[25] Substantial effort has been focused on the chemistry of growing single chirality tubes with high temperature (>500 °C) vapor deposition.[26] These SWNTs may be transferred subsequently to flexible substrates,[27] but the scaling of this method with flexible large-area substrates remains unclear. Bulk chirality separation methods include dielectrophoresis,[28] macromolecular/DNA wrapping,[29] and selective reactions,[30−32] yet the yield is relatively low and it remains unclear how these methods ultimately affect SWNT electronic properties. In another approach, researchers have adopted a technique from biochemistry and demonstrated separation by density gradient centrifugation,[33,34] and this appears to be promising for scalable device integration provided the surfactants/centrifuge medium can be completely removed and not alter TFT properties.[35] Meanwhile, device structure engineering by patterning etch lines into SWNT networks long-channel devices (100 μm) was demonstrated to cut off percolation paths of metallic SWNTs, but this imposes restrictions on the final device dimensions.[10]

We have been focusing efforts to address the above issues of SWNT separation and alignment by developing a solution-based fabrication method for SWNTntTFTs with the ability to control the chirality and topological characteristics. This approach not only provides a modular platform toward the fabrication of SWNT-based electronics but also allows us to understand how the topological characteristics, namely, density and alignment, affect the transistor performance. Our previously demonstrated approach,[36] which relies upon specific (noncovalent) interfacial interactions to enrich SWNT chirality, is advantageous here since it contains multiple deposition parameters (surface chemistry, spin rate, concentration, solution volume, *etc.*) to simultaneously tune network alignment and density. We incorporate a single-step process directly on a gate/insulator substrate resulting in a refined SWNT network film immediately viable for flexible electronic applications. We have applied this to both SiO_2 and flexible polymeric and ITO substrates. On SiO_2 modified with amine or aromatic functionality, the resulting networks possess very different levels of alignment and density under the same deposition conditions, with on/off ratio averaging around 100 000 and 1.2, respectively.[36] The SWNTntTFTs on polymeric and ITO substrates had slightly lower on/off ratio (10^3) due to increased surface roughness, yet high enough performance and stability to function as underwater, low-voltage TFTs.[37] We used aminosilanes due to their well-known affinity to CNTs, which has been shown to selectively bind SC−SWNTs.[31,36] Here, the deposition parameters, including spin rate and SWNT solution volume, are systemically varied to control the SWNT density and alignment, and the influence of these properties on the electrical performance is reported. Our results demonstrate how the interplay between density and alignment can be used to tune the electrical performance of solution-assembled SWNTntTFTs.

RESULTS AND DISCUSSION

SWNT Network Formation. SWNTnts were fabricated from arc-discharge SWNTs in *n*-methyl pyrrolidone (NMP) solutions spin-coated onto amine-functionalized substrates with variable spin-coating speeds, as depicted in Figure 1. The conditions have been described in detail previously[36] (see also Materials and Methods), but briefly, we used well-dispersed and debundled SWNT/NMP solutions (10 μg/mL), as this solvent has been shown to completely exfoliate CNTs into SWNTs.[38] Furthermore, surfactants are not used in this process as these can alter SWNT electronic properties. Using silane chemistry, the surface of a Si/SiO_2 substrate was functionalized with an amine-terminated monolayer for reasons described previously. The selective adsorption process is critical on having a smooth and close-packed amine layer, with water contact angle above 40°. Aminosilane monolayer formation from APTES is nontrivial, as suggested by the large range of contact angles (from 23 to 93°) reported in the literature, due to the high environmental sensitivity of amine-containing silanes.[39,40] In addition to the triethoxysilane headgroup assembling along the SiO_2 surface, a variety of undesirable interactions can occur to disrupt the formation of a uniform monolayer. Amine groups can hydrogen bond to the surface, or with a sufficient amount of water in the system (a small amount is required for the hydrolysis reaction), the amine monomer can polymerize in the solution resulting in rough surfaces with large aggregates of silane deposits.[41] Excessive reaction times can also lead to high contact angle with high surface roughness due to multilayer formation.[39,42] These undesirable reaction attributes lead to the large range in contact angles and film thicknesses; however, we have found that aminosilane monolayers with contact angle between 38 and below 80° can be suitable for our deposition/separation process (Supporting Information).

Using amine-terminated substrates prepared in the same APTES deposition batch with contact angles of around 60°, samples were fabricated according to the spin-coating and SWNT solution volume conditions described in Table 1. Overall, the alignment listed in Table 1 deviated not more than ±2% for all substrates (four

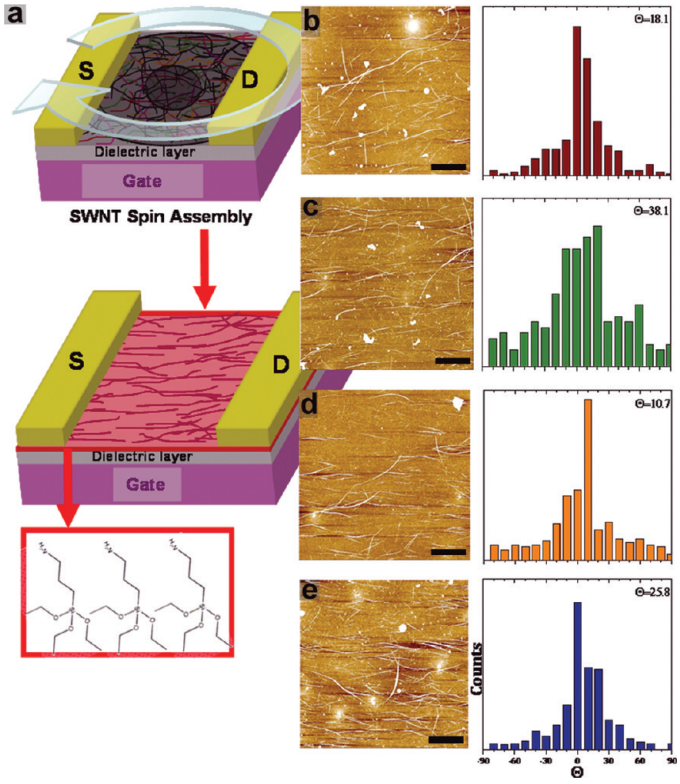

Figure 1. (a) Schematic depicting assembly of the SWNTnt formation. The SWNT solution (10 μg/mL in NMP) is spin-coated onto the amine-functionalized dielectric, followed by deposition of source and drain electrodes. (b−e) Resulting AFM images (10 × 10 μm, *z*-scale is 10 nm) of the SWNTnt deposited under the different conditions described in Table 1, as well as the corresponding alignment histograms where Θ is the fwhm value of the Gaussian fit to the histograms. From top to bottom are A1 (b), A2 (c), A3 (d), and A4 (e). The scale bar in b−e is 2 μm.

tested) within each sample type, indicating good reproducibility of this method. In order to gain a better understanding of how topology affects the electrical performance of SWNTntTFTs, here we prepared films by varying the spin rate, which affects alignment and SWNT density (solution volume). The average alignment of networks deposited with 50 μL solution at 2000 rpm was determined from 10 × 10 um^2 AFM images recorded from at least four locations over the entire substrate (2.5 cm long by 1.5 cm wide), indicating that roughly 71% of the SWNTs are aligned within ±10% away from the long axis of the substrate (histograms, Figure 1b). Neither preferential alignment nor absorption was observed, resulting in no transistor behavior when networks were assembled at a slower spin rate of 1000 rpm (Supporting Information). Apparently, the shear rate is not high enough to enable selective adsorption. Networks deposited with a larger volume of solution (100 μL) at 2000 rpm displayed poor alignment (55% within ±10%) owing to the SWNTs in solution interacting more with the nascent SWNTs on the surface rather than the underlying amine monolayer. The effect of a faster spin rate is significant, whereby 75% of the SWNTs are aligned within ±10% when depositing 50 μL SWNT solution at 4000 rpm. Even when using the large volume (100 μL) at 4000 rpm, a reasonably high alignment is still achieved (69%) relative to that observed with the same volume (100 μL) at 2000 rpm (55%).

Electrical Properties. As evidenced from Figure 1 and summarized in Table 1, regular arrays of SWNTnt are fabricated with various topologies. To understand how the topology effects electronic properties, we deposited top contact source/drain gold electrodes with L_C = 50 μm and W = 1000 μm (on 300 nm SiO_2) and measured the TFT characteristics. The resulting transfer plots are shown in Figure 2 (see Supporting Information for corresponding output curves). Gate leakage in all tested devices did not exceed 10 pA. From the averaged semilog transfer plots (Figure 2), it is difficult to accurately determine the threshold voltage (V_T), particularly due to the spread in V_T arising from the presence of various SWNT, substrate interactions, SWNT/electrode contact, and SWNT/SWNT interactions.[35,43] In fact, by measuring devices at very small channel lengths (*e.g.*, L_C = 2 μm; see Figure 3 and Figure SI-4), where there is typically only a few, if not a single, SWNT, these off-state current/V_T variations, which are highly sensitive to band gap energy (a function of slight variations in diameter), could be observed.

For electronic measurements, results were averaged from four substrates for each sample type. Over-

TABLE 1. Samples Described in Figure 1[a]

sample type	spin-coat RPM	spin-coat volume (μL)	SWNT density (tubes/μm^2)	avearge SWNT alignment (%) within ±10%	gate modulation	max I_{DS}current (μA)	average mobility (cm^2/(V · s))	average on/off
A0[b]	1000	50	7	40	no	1.22	NA	1.97
A1	2000	50	8	71	yes	0.10	0.5	1.13 × 10^5
A2	2000	100	12	55	yes	0.80	11	246
A3	4000	50	7	75	yes	0.19	1.1	1.34 × 10^5
A4	4000	100	11	69	yes	0.24	2.0	4.62 × 10^5

[a]Substrate size is 2.5 cm long, 1.5 cm wide. Four substrates of each type were examined. APTES contact angle is 60° for all samples, and SWNT solution (10 μg/mL in NMP) was dispensed at the center of the substrate. L_C = 50 μm, W_C = 1000 μm. [b]See the Supporting Information.

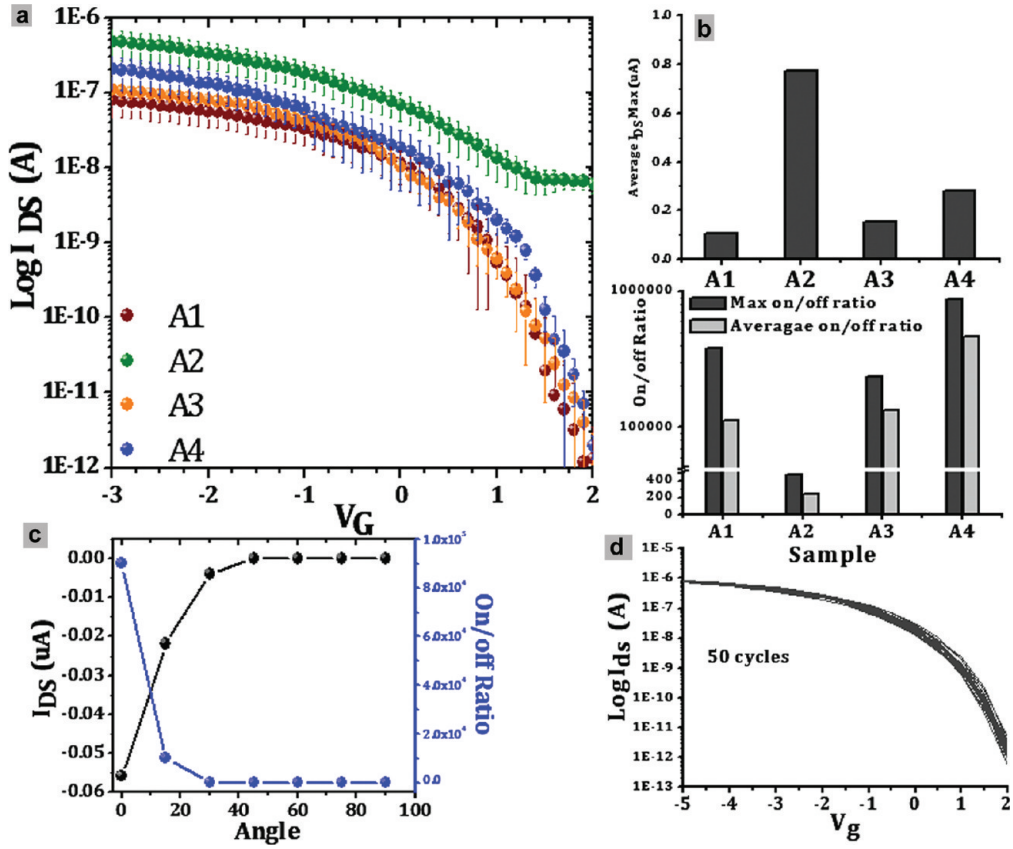

Figure 2. (a) Transfer characteristics ($I_{DS}-V_G$) for each of the SWNTnts. These are averaged from tests done on eight devices ($L_C = 50$ μm, $W_C = 1000$ μm) on four different wafers for each condition at $V_{DS} = -1$ V (32 devices for each condition). (b) Histograms compiled from the transfer characteristics showing average I_{DS} max, as well as comparing the average and maximum values for on/off ratio. (c) Typical angular dependence of the SWNTnt for sample type A4. This type of test demonstrates the high alignment of SWNTnt, and when source/drain electrodes ($L_C = 5$ μm, $W_C = 500$ μm) are deposited more than 20° perpendicular from the direction of SWNT alignment, the transistors are "off" (no gating). (d) Typical cycling (transfer characteristics) (at $V_{DS} = -1$ V) for sample A4 over 50 cycles on a devices with $L_C = 50$ μm, $W_C = 1000$ μm.

all, on/off ratio reached a maximum value of nearly 9 $\times 10^5$ (Figure 2), and all samples exhibited on/off ratios of over 10^5. The level of mobility is lower than typically observed in CVD-grown networks, and this can be attributed to the increased defects in SWNTs due to extensive solution processing. The poorest performing sample type was A2 (2K, 50 μL), which also had the poorest alignment. The poor TFT performance of sample A2 is a result of large MET−SWNT content, evidenced by an order of magnitude higher "on-current" and more than 4 orders of magnitude higher "off-currents". Greater MET−SWNT content is also observed by Raman spectroscopy results (discussed later). When comparing this result relative to sample A4, in which the overall SWNTnt density is the same, the importance of higher spin speed becomes clear. The higher fluidic shear force leads to enhanced alignment, in addition to chirality enrichment. In other words, at a spin speed of 2000 rpm, the selective tube/surface interaction breaks down after 50 μL of deposited solution, corresponding to a density of $>9/\mu m^2$, as the inefficient packing of SWNTs increases effective coverage and lowers the surface area of the free amine layer. In this case, an increase in nanotube density is not possible, but rather SWNTs nonspecifically adsorb to the existing network resulting in degraded TFT behavior. However, at a spin speed of 4000 rpm, because of the higher alignment, the density of SWNTs can be increased with an enhancement of TFT behavior.

Comparing sample types A3 (4K, 50 μL) and A4 (4K, 100 μL), essentially doubling the SWNT concentration does not drastically affect alignment and results in both an increased on/off ratio and on-current, with an $I_{DS\text{-}max}$ of A4 double that of A3. The SWNTnt alignment is significantly better in A3 (75%) than A4 (69%). Thus, the lower I_{DS} current makes sense because typically a higher level of alignment produces a slightly lower on/off ratio due to a lower on-current ($I_{DS\text{-}max}$) caused by a lower number of percolation paths. From a qualitative perspective, a small level of misalignment is necessary for TFT networks of 1D nanostructures, and quantitatively, it appears that optimum charge transport in terms of the highest max on/off ratio (Figure 1) is achieved when 70% of tubes are within ±90% parallel with each other. Furthermore, although A1 (2K, 50 μL) and A3 (4K, 50 μL) have the same relative density, the $I_{DS\text{-}max}$ current is lower for A1, most likely due to the large level of misalignment leading to more tube/tube contacts causing

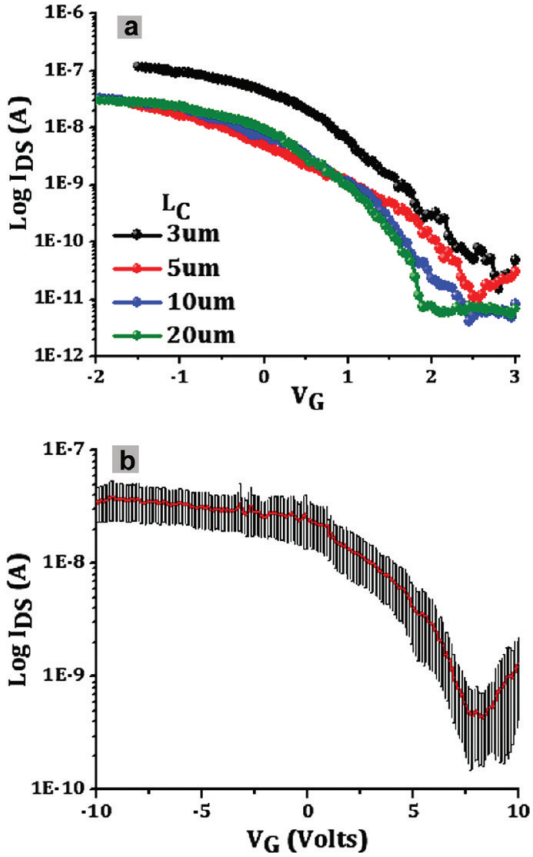

Figure 3. (a) Transfer characteristics at smaller channel lengths. While V_T is affected strongly going to smaller L_C (W_C kept constant at 100 μm) due to a lower number of tubes being sampled, the on/off ratio remains relatively constant ($V_{DS} = -1$ V). (b) Average transfer characteristics at $L_C = 2$ μm, $W_C = 2$ μm ($V_{DS} = -1$ V, averaged over 20 devices). Even with such a small channel geometry where perhaps one percolation path is present, on/off ratio remains over 100, with on-current (I_{DS} max) being reduced due to the low number of SWNTs being sampled.

increased channel resistance. The high level of alignment that can be achieved is revealed in Figure 2c in which devices ($L_C = 5$ μm, $W = 50$ μm) tested that were perpendicular to the direction of alignment by only more than 20° became insulating. Moreover, in terms of reliability, the SWNT TFTs fabricated here have very low hysteresis measured in air (Figure 2d), indicating these devices are highly stable in ambient, and APTES is suitable for passivating the trap states on the SiO_2 surface. While the mobility of these solution-processed devices is low compared to SWNT TFTs made with CVD[44] or prepurified[35] SWNTs, this value is still on par with published results.[16,18,45] However, the on/off ratios reported here are nearly 2 orders of magnitude better than those obtained previously with solution-processed nanotube networks. This combination of results is quite significant for nanotube networks fabricated directly from solution, as opposed to multistep processed or high-temperature CVD fabricated nanotube networks.

Finally, the on/off ratio did not significantly decrease going to smaller channel lengths, an indication

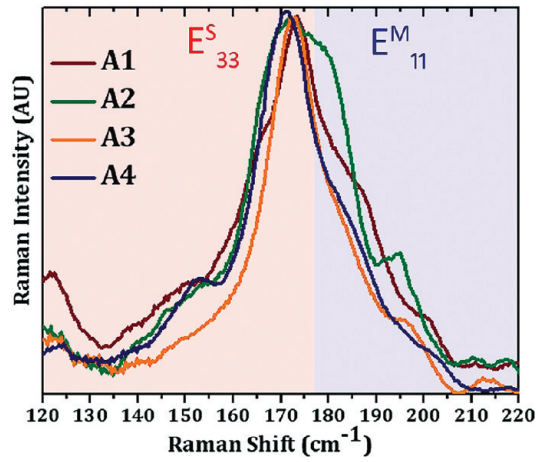

Figure 4. μ-Raman mapping data at 633 nm (1.96 eV excitation). The resulting spectrum for each sample is averaged over four maps (12 point mapping over a 200 × 200 μm area) on four different substrates for each condition. The curves are normalized to the largest RBM peak (~170 cm^{-1}) for direct comparison. The blue shaded region represents the metallic tubes, while the red shaded region represents the semiconducting tubes resonant at this wavelength.

of true SC−SWNT enrichment in the network. Figure 3 shows the result of testing small channel devices as described above with density of tubes around 8/μm^2. In Figure 3a, devices were fabricated at $L_C = 3$, 5, 10, and 20 μm, with W_C constant at 100 μm, and the results shown were averaged over 10 devices for each channel length. The average on/off ratio remains around 10^4, but importantly, off-current does not exceed 0.1 nA. As expected, average mobility is slightly affected by channel length as 3 μm is highest, before dropping off and remaining at a constant level for 5−20 μm (mobility at 3 μm is better than at 2 μm because the 2 μm devices had lower W/L as $W_C = 2$ μm for $L_C = 2$ μm). Interestingly, V_T steadily increases from 1.9 to 2.9 V with decreasing channel length, indicative of a lower sampling of SWNTs (see above) species having their properties averaged as L_C decreases. At smaller channel dimensions, these outliers (either a very small percentage of MET−SWNTs or small diameter, smaller band gap SC−SWNTs) become statistically significant, especially on the 2 × 2 μm devices.

μ-Raman Analysis. An overall comparison of the μ-Raman results at 1.96 eV excitation for all samples is summarized in Figure 4. The 1.96 eV excitation energy is resonant with the majority of SWNT tubes used in this work, which possess a relatively large average diameter of 1.4 ± 0.5 nm, determined by AFM. In particular, the 1.96 eV line is well-suited for separation analysis because it is resonant with MET−SWNT (E^M_{11}) and SC−SWNT (E^S_{33}) in a nearly 50/50 ratio as indicated in Figure 4 by the blue and red shaded regions, respectively. As discussed before, sample A2 exhibited the poorest transistor behavior likely due to the presence of MET−SWNTs manifested in the relatively high off-current compared to other samples. Focusing on the

TABLE 2. Samples Described in Figure 5[a]

sample type	spin-coat RPM	spin-coat volume (μL)	SWNT density (tubes/μm²)	average SWNT alignment (%) within ±10%	gate modulation	max I_{DS} current (μA)	average mobility (cm²/(V · s))	average on/off
0	4000	25	3	76	no	insulating	NA	N/A
1	4000	50	5	78	yes	0.05	0.9	1.4×10^4
2	4000	100	11	71	yes	0.16	1.4	1.2×10^5
3	4000	150	15	69	yes	0.20	1.9	2.2×10^5
4	4000	175	18	69	yes	4.11	17	2.8×10^2
5	4000	200	22	67	no	6.90	NA	NA

[a]Substrate size is 2.5 cm long, 1.5 cm wide. Three substrates of each type were examined. APTES contact angle is 60° for all samples, and SWNT solution (10 μg/mL in NMP) was dispensed at the center of the substrate. $L_C = 50$ μm, $W_C = 1000$ μm.

low-frequency radial breathing mode (RBM) region of the spectra, which reveals SWNT chirality determined through methods described previously,[46,47] it is clear that A2 (2K, 100 μL) has a larger and broader shoulder at the high-end frequencies as compared to the other samples with more SC-enriched networks. In fact, the average spectrum for A2 is bimodal (Figure 4 and Supporting Information), indicating little enrichment of SC−SWNTs. It is apparent that, for sample A2, the assembly leading to poor alignment from insufficient SWNT/surface interaction does lead to a deposition of a SWNTnt with a mixed chirality content and with charge transport properties dominated by MET−SWNTs.

As expected, all samples show a strong SC band at roughly 170 cm^{-1} because SC−SWNTs are initially selectively adsorbed in the assembly process. However, samples A1 and A2 have a larger RBM area in the blue shaded region (Figure 4) compared to A3 and A4, and this is a result of the stronger hydrodynamic force during network assembly, resulting in better selectivity for A3 and A4. While sample A1 has a noticeable MET−SWNT peak, this is still much smaller than the nearly bimodal distribution for sample A2, and this explains the better on/off ratio for sample A1 relative to A2. Furthermore, the lower SWNT density of A1 relative to A2 (Figure 1 and Table 1) leads to less metallic percolation paths in the network, but this should also reduce I_{DS} current; this is observed in the electronic performance (Figure 2b), where A2 had the lowest current. Thus, the Raman data corroborate the electronic and AFM data. Looking at the average RBM spectra for samples A3 and A4, smaller MET−SWNT content is detected relative to A1 and A2, with just very small shoulders at ~200 cm^{-1}. We therefore conclude that, at slower spin rates, the network is very sensitive to density for achieving high on/off ratio as observed from combined electrical and spectroscopic characterization. With faster spin-coating speed, the binding at the aminosilane interface is more selective, and the on/off ratio is not sensitive to density until higher values are reached (see below). At higher spin rates, the nanotubes have a shorter residence time with the substrates and are less likely to be absorbed by weak, nonspecific interactions.

SWNT Density Influence on Sorting. At a spin speed of 2000 rpm, the electrical performance of SWNTntTFTs breaks down at an accumulation density of just over 10 tubes/μm². At faster spin rates, however, a critical breakdown density point was not reached for the aforementioned system. To this end, the maximum SWNT density was determined by gradually increasing the volume of deposited solution while maintaining a constant spin rate of 4000 rpm, according to the samples listed in Table 2. Figure 5 shows AFM topography images of network arrays with increasing SWNT density, from insulating networks with low density up to highly conductive, dense networks on the verge of selective absorption breaking down in which no significant gating was observed. The corresponding transfer curves (averaged from 24 individual curves over three samples for each density) demonstrate that the electronic properties are heavily influenced by SWNT density.

This is summarized in Figure 6, where the on/off ratio and mobility steadily increase until about 15 SWNTs/μm². At this point, the on/off ratio falls off dramatically, while the $I_{DS\text{-}max}$ continues to increase. The optimal nanotube density is indicated by the green (center) shaded region in Figure 6, where high charge transport is accompanied by reasonably high on/off ratio, which apparently is around 14−18 tubes/μm². Looking at sample 4, although the on/off ratio remains above 100, this value represents a sharp drop (3 orders of magnitude) from the previous samples as a result of surface sorting breaking down. The incoming SWNTs begin to have more interaction with the nascent SWNT network rather than "empty" surface, resulting in nonspecific adsorption. This is reflected in an order of magnitude increase in current for sample 4 as well as an off-current that jumps from picoamperes to tens of nanoamperes. Because of this, the corresponding mobility is increased by nearly an order of magnitude. Simply put, this is due to the presence of more MET−SWNTs. It should be noted that when going to faster spin assembly speeds (greater than 4K), electronic perfor-

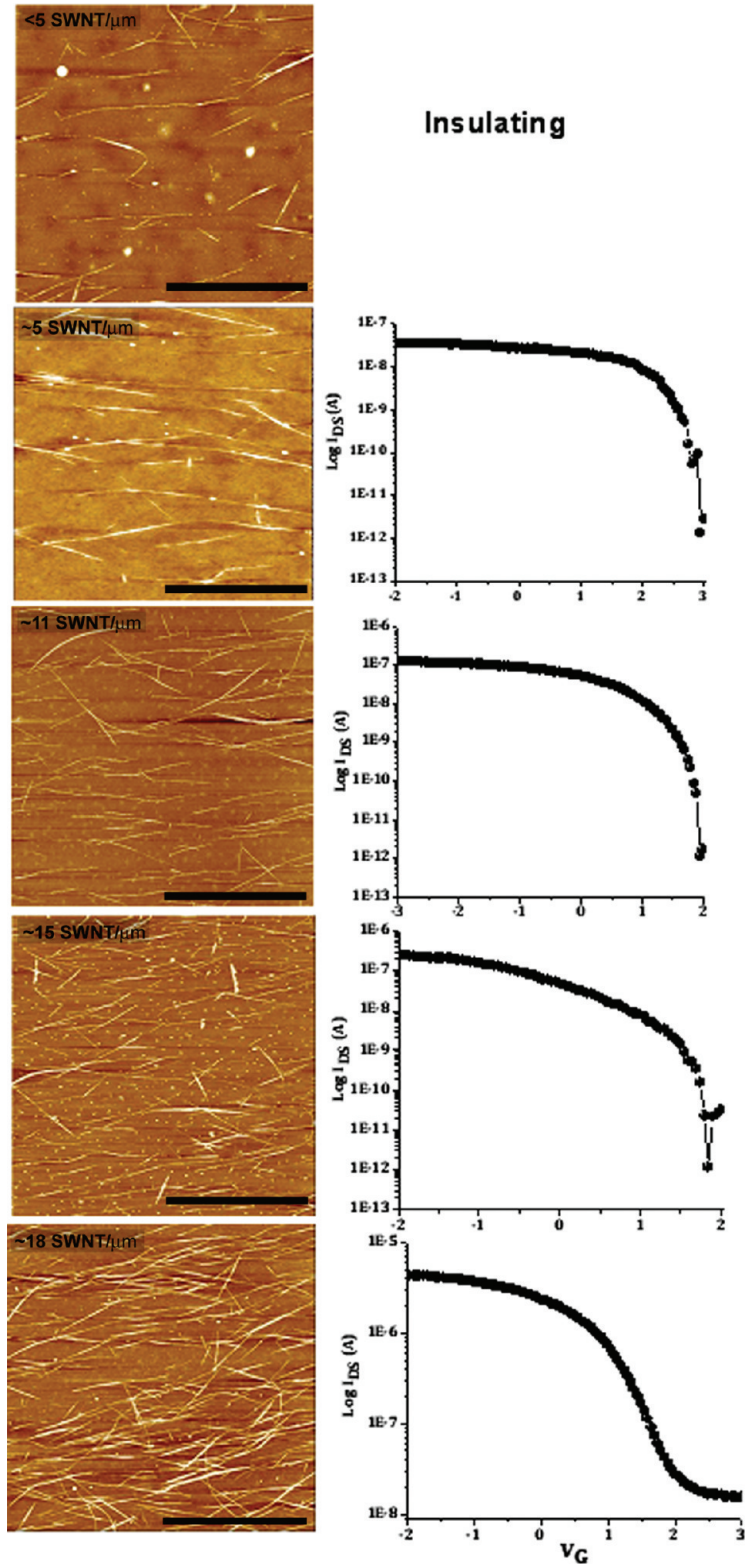

Figure 5. Series of typical AFM images (2 × 2 μm, *z*-scale = 10 nm) of the SWNT networks at each density indicated, with increasing density from top to bottom. The scale bar represents 1 μm. The right column is the average transfer characteristics at each density (L_C = 50 μm, W_C = 1000 μm, V_{DS} = −1 V) over eight devices from three substrates at each condition.

mance did not improve because alignment becomes dramatically enhanced resulting in much reduced tube/tube contacts. This higher alignment regime leads to very low I_{DS} current, as can be seen in Figure S-6 in the Supporting Information. Further studies are being carried out on the properties of aligned CNTs in this regime and this will be the subject of another publication.

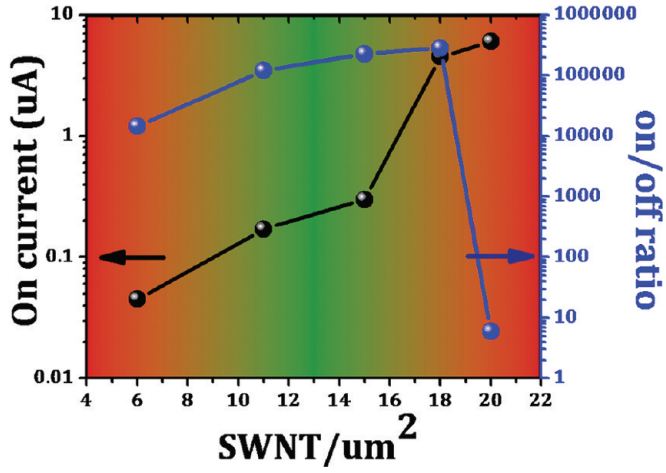

Figure 6. Compilation plot of the transfer characteristics as a function of density. This shows that the I_{DS} max is steadily increasing, while on/off ratio reaches a maximum value at around 16 tubes/μm^2, indicating that the surface sorting begins to breakdown at this tube density.

In conclusion, nanotube networks are important electronic materials, and a full understanding of their electronic properties, which is heavily dependent upon network topology, will be required for potential TFT device integration. In this work, an approach to thin-film transistor development of going beyond "random" nanotube network devices with a self-sorted SWNTnt is expanded upon here. The characterization of these SWNTnts in terms of electronic properties as a function of network topology has not been investigated for these critical systems made from a scalable, one-step solution process. The performance of SWNTntTFTs is dramatically altered by tube density, alignment, and spin-coating speed, all of which can be easily tuned with our process. μ-Raman mapping indicates more efficient specific chirality sorting at a spin speed of 4k as opposed to 2k, and by looking at a wide range of samples, there is a "sweet-spot" for devices that combine higher I_{DS} max with higher on/off ratio. By gaining an insight into the hydrodynamic/surface binding force balance at this crucial interface, this can pave the way for a powerful, one-step solution-based process that is scalable and applicable to plastic (flexible) and metal surfaces.

MATERIALS AND METHODS

Preparation of Surfaces. Doped silicon wafers (Silicon Quest) of (100) orientation with 300 nm oxide were cleaned for 30 min in Piranha solution (3:1 H_2SO_4/H_2O_2), rinsed copiously with water, dried under N_2, and taken inside a dry N_2 glovebox for silane modification. SAMs of aminopropyltriethoxy silane (APTES) (Gelest, silanes were distilled prior to use) were absorbed from 0.5% solution (in anhydrous toluene) for reaction times ranging from 5 min to 2 h at room temperature. Following self-assembly, surfaces were rinsed twice in toluene, sonicated in toluene, and rinsed again in toluene, then dried under N_2, annealed under vacuum for 20 min at 90 °C before characterization. SAM surface roughness did not exceed 0.3 nm rms measured with AFM. TFT geometry for bottom contact devices was achieved through conventional lithography, 40 nm thick gold electrodes); L_C = 2, 5, 10, 25, and 50 μm, while W_C = 2, 50, or 100 μm. Top contact source/drain electrodes deposited from 40 nm gold through a shadow mask, with L_C = 50 μm and W_C = 1000 μm.

Nanotube Solution Preparation. Details of the nanotube purification and resulting "buckypaper" formation are provided in a previous publication.[36] Solutions of the purified buckypaper were prepared by dissolving small amounts of buckypaper (by 20 min of sonication at 700 W, 60% amplitude) at a concentration of 10 μg/mL in NMP (1-methyl-2-pyrrolidone, Omnisolve, spectrophotometry grade).

Spin-Coating Procedure. These solutions were carefully dropped *via* pipet near the surface and in the center of a 2.5 cm × 1.5 cm of the APTES-modified silicon wafer spinning at speeds between 500 and 6000 rpm (Headway research).

Sample Characterization. AFM topography images were acquired in the tapping mode regime using a Multimode AFM (Veeco). Alignment and density analysis was carried out with ImageJ software. All electronic tests were conducted using a Keithley 4200 SC semiconductor analyzer. μ-Raman (LabRam Aramis, Horiba Jobin Yvon) measurements were carried out at 633 nm (1.96 eV) excitation at 100× magnification and 1 μm spot size, and 1800 grating. Excitation power through our filter was 2 mW for the 633 nm line. All data were acquired from automated multipoint (12 points) mapping over random areas (at least five different areas) of the samples, with three spectra accumulated and averaged at each single point. All summarized data were normalized to the 303 cm^{-1} mode in silicon.

Acknowledgment. This research was supported by the Stanford Global Climate & Energy Program (GCEP), the NSF sponsored Center for Polymer Interface and Macromolecular Assemblies (CPIMA), Samsung Advanced Research Institute, and Intel. M.C.L. acknowledges support from the Intelligence Community Postdoctoral Fellowship Program. M.R. acknowledges support from the NASA Graduate Student Research Fellowship, and J.P.O. acknowledges support from a Stanford Graduate Fellowship. Z.B. acknowledges support from a Sloan Research Fellowship.

Supporting Information Available: Additional surface conditions and additional SWNT network deposition conditions and resulting electronic properties, as well as additional μ-Raman spectra of the RBM regions. This material is available free of charge *via* the Internet at http://pubs.acs.org.

REFERENCES AND NOTES

1. Mamedov, A. A.; Kotov, N. A.; Prato, M.; Guldi, D. M.; Wicksted, J. P.; Hirsch, A. Molecular Design of Strong Single-Wall Carbon Nanotube/Polyelectrolyte Multilayer Composites. *Nat. Mater.* **2002**, *1*, 190–194.
2. Lovat, V.; Pantarotto, D.; Lagostena, L.; Cacciari, B.; Grandolfo, M.; Righi, M.; Spalluto, G.; Prato, M.; Ballerini, L. Carbon Nanotube Substrates Boost Neuronal Electrical Signaling. *Nano Lett.* **2005**, *5*, 1107–1110.
3. Star, A.; Han, T.-R.; Gabriel, J.-C. P.; Bradley, K.; Gruener, G. Interaction of Aromatic Compounds with Carbon Nanotubes: Correlation to the Hammett Parameter of the Substituent and Measured Carbon Nanotube Fet Response. *Nano Lett.* **2003**, *3*, 1421–1423.
4. Novak, J. P.; Snow, E. S.; Houser, E. J.; Park, D.; Stepnowski, J. L.; McGill, R. A. Nerve Agent Detection Using Networks of Single-Walled Carbon Nanotubes. *Appl. Phys. Lett.* **2003**, *83*, 4026–4028.
5. Lee, C. Y.; Strano, M. S. Understanding the Dynamics of Signal Transduction for Adsorption of Gases and Vapors on Carbon Nanotube Sensors. *Langmuir* **2005**, *21*, 5192–5196.
6. Wang, F.; Gu, H.; Swager, T. M. Carbon Nanotube/Polythiophene Chemiresistive Sensors for Chemical Warfare Agents. *J. Am. Chem. Soc.* **2008**, *130*, 5392–5393.

7. Rowell, M. W.; Topinka, M. A.; McGehee, M. D.; Prall, H.-J.; Dennler, G.; Sariciftci, N. S.; Hu, L.; Gruner, G. Organic Solar Cells with Carbon Nanotube Network Electrodes. *Appl. Phys. Lett.* **2006**, *88*, 233506/233501–233506/233503.
8. Camacho, R.; Morgan, A.; Flores, M.; McLeod, T.; Kumsomboone, V.; Mordecai, B.; Bhattacharjea, R.; Tong, W.; Wagner, B.; Flicker, J.; Turano, S.; Ready, W. Carbon Nanotube Arrays for Photovoltaic Applications. *J. Met., Mater. Miner.* **2007**, *59*, 39–42.
9. Ryu, K.; Badmaev, A.; Wang, C.; Lin, A.; Patil, N.; Gomez, L.; Kumar, A.; Mitra, S.; Wong, H. S. P.; Zhou, C. Cmos-Analogous Wafer-Scale Nanotube-on-Insulator Approach for Submicrometer Devices and Integrated Circuits Using Aligned Nanotubes. *Nano Lett.* **2009**, *9*, 189–197.
10. Cao, Q.; Kim, H.-s.; Pimparkar, N.; Kulkarni, J. P.; Wang, C.; Shim, M.; Roy, K.; Alam, M. A.; Rogers, J. A. Medium-Scale Carbon Nanotube Thin-Film Integrated Circuits on Flexible Plastic Substrates. *Nature* **2008**, *454*, 495–500.
11. Lee, C. Y.; Scharma, R.; Radadia, A. D.; Masel, R. I.; Strano, M. S. On-Chip Micro Gas Chromatograph Enabled by a Noncovalently Functionalized Single-Walled Carbon Nanotube Sensor Array. *Angew. Chem., Int. Ed.* **2008**, *47*, 5018–5021.
12. Green, A. A.; Hersam, M. C. Colored Semitransparent Conductive Coatings Consisting of Monodisperse Metallic Single-Walled Carbon Nanotubes. *Nano Lett.* **2008**, *8*, 1417–1422.
13. Hellstrom, S. L.; Lee, H. W.; Bao, Z. Polymer-Assisted Direct Deposition of Uniform Carbon Nanotube Bundle Networks for High Performance Transparent Electrodes. *ACS Nano* **2009**, *3*, 1423–1430.
14. Fanchini, G.; Miller, S.; Parekh, B. B.; Chhowalla, M. Optical Anisotropy in Single-Walled Carbon Nanotube Thin Films: Implications for Transparent and Conducting Electrodes in Organic Photovoltaics. *Nano Lett.* **2008**, *8*, 2176–2179.
15. Javey, A.; Guo, J.; Wang, Q.; Lundstrom, M.; Dai, H. Ballistic Carbon Nanotube Field-Effect Transistors. *Nature* **2003**, *424*, 654–657.
16. Snow, E. S.; Novak, J. P.; Campbell, P. M.; Park, D. Random Networks of Carbon Nanotubes as an Electronic Material. *Appl. Phys. Lett.* **2003**, *82*, 2145–2147.
17. Kocabas, C.; Kang, S. J.; Ozel, T.; Shim, M.; Rogers, J. A. Improved Synthesis of Aligned Arrays of Single-Walled Carbon Nanotubes and Their Implementation in Thin Film Type Transistors. *J. Phys. Chem. C* **2007**, *111*, 17879–17886.
18. Artukovic, E.; Kaempgen, M.; Hecht, D. S.; Roth, S.; Gruner, G. Transparent and Flexible Carbon Nanotube Transistors. *Nano Lett.* **2005**, *5*, 757–760.
19. Kumar, S.; Pimparkar, N.; Murthy, J. Y.; Alam, M. A. Theory of Transfer Characteristics of Nanotube Network Transistors. *Appl. Phys. Lett.* **2006**, *88*, 123505.
20. Kocabas, C.; Pimparkar, N.; Yesilyurt, O.; Kang, S. J.; Alam, M. A.; Rogers, J. A. Experimental and Theoretical Studies of Transport through Large Scale, Partially Aligned Arrays of Single-Walled Carbon Nanotubes in Thin Film Transistors. *Nano Lett.* **2007**, *7*, 1195–1202.
21. Buldum, A.; Lu, J. P. Contact Resistance between Carbon Nanotubes. *Phys. Rev. B* **2001**, *63*, 161403.
22. Fuhrer, M. S.; Nygård, J.; Shih, L.; Forero, M.; Yoon, Y.-G.; Mazzoni, M. S. C.; Choi, H. J.; Ihm, J.; Louie, S. G.; Zettl, A.; McEuen, P. L. Crossed Nanotube Junctions. *Science* **2000**, *288*, 494–497.
23. Avouris, Ph.; Chen, Z.; Perebeinos, V. Carbon-Based Electronics. *Nat. Nanotechnol.* **2007**, *2*, 605–615.
24. Qing Cao, J. A. R. Ultrathin Films of Single-Walled Carbon Nanotubes for Electronics and Sensors: A Review of Fundamental and Applied Aspects. *Adv. Mater.* **2009**, *21*, 29–53.
25. Collins, P. G.; Arnold, M. S.; Avouris, P. Engineering Carbon Nanotubes and Nanotube Circuits Using Electrical Breakdown. *Science* **2001**, *292*, 706–709.
26. Li, Y.; Mann, D.; Rolandi, M.; Kim, W.; Ural, A.; Hung, S.; Javey, A.; Cao, J.; Wang, D.; Yenilmez, E.; Wang, Q.; Gibbons, J. F.; Nishi, Y.; Dai, H. Preferential Growth of Semiconducting Single-Walled Carbon Nanotubes by a Plasma Enhanced CVD Method. *Nano Lett.* **2004**, *4*, 317–321.
27. Meitl, M. A.; Zhou, Y.; Gaur, A.; Jeon, S.; Usrey, M. L.; Strano, M. S.; Rogers, J. A. Solution Casting and Transfer Printing Single-Walled Carbon Nanotube Films. *Nano Lett.* **2004**, *4*, 1643–1647.
28. Krupke, R.; Hennrich, F.; Loehneysen, H. V.; Kappes, M. M. Separation of Metallic from Semiconducting Single-Walled Carbon Nanotubes. *Science* **2003**, *301*, 344–347.
29. Zheng, M.; Jagota, A.; Semke, E. D.; Diner, B. A.; McLean, R. S.; Lustig, S. R.; Richardson, R. E.; Tassi, N. G. DNA-Assisted Dispersion and Separation of Carbon Nanotubes. *Nat. Mater.* **2003**, *2*, 338–342.
30. Strano, M. S. Carbon Nanotubes: Sorting out Left from Right. *Nat. Nanotechnol.* **2007**, *2*, 340–341.
31. Chattopadhyay, D.; Galeska, I.; Papadimitrakopoulos, F. A Route for Bulk Separation of Semiconducting from Metallic Single-Wall Carbon Nanotubes. *J. Am. Chem. Soc.* **2003**, *125*, 3370–3375.
32. Lu, J.; Lai, L.; Luo, G.; Zhou, J.; Qin, R.; Wang, D.; Wang, L.; Mei, W. N.; Li, G.; Gao, Z.; Nagase, S.; Maeda, Y.; Akasaka, T.; Yu, D. Why Semiconducting Single-Walled Carbon Nanotubes Are Separated from Their Metallic Counterparts. *Small* **2007**, *3*, 1566–1576.
33. Arnold, M. S.; Green, A. A.; Hulvat, J. F.; Stupp, S. I.; Hersam, M. C. Sorting Carbon Nanotubes by Electronic Structure Using Density Differentiation. *Nat. Nanotechnol.* **2006**, *1*, 60–65.
34. Arnold, M. S.; Stupp, S. I.; Hersam, M. C. *Nano Lett.* **2005**, *5*, 713–718.
35. Engel, M.; Small, J. P.; Steiner, M.; Freitag, M.; Green, A. A.; Hersam, M. C.; Avouris, Ph. Thin Film Nanotube Transistors Based on Self-Assembled, Aligned, Semiconducting Carbon Nanotube Arrays. *ACS Nano* **2008**, *2*, 2445–2452.
36. LeMieux, M. C.; Roberts, M.; Barman, S.; Jin, Y. W.; Kim, J. M.; Bao, Z. Self-Sorted, Aligned Nanotube Networks for Thin-Film Transistors. *Science* **2008**, *321*, 101–104.
37. Mark, E.; Roberts, M. C. L. Anatoliy Sokolov, Zhenan Bao. *ACS Nano* 2009.
38. Bergin, S. D.; Nicolosi, V.; Streich, P. V.; Giordani, S.; Sun, Z.; Windle, A. H.; Ryan, P.; Niraj, N. P. N.; Wang, Z.-T.; Carpenter, L.; *et al.* Towards Solutions of Single-Walled Carbon Nanotubes in Common Solvents. *Adv. Mater.* **2008**, *20*, 1876–1881.
39. Howarter, J. A.; Youngblood, J. P. Optimization of Silica Silanization by 3-Aminopropyltriethoxysilane. *Langmuir* **2006**, *22*, 11142–11147.
40. Siquiera Petri, D. F.; Wenz, G.; Schunk, P.; Schimmel, T. *Langmuir* **1999**, *15*, 4520.
41. Vandenberg, E. T.; Bertilsson, L.; Liedberg, B.; Uvdal, K.; Erlandsson, R.; Elwing, H.; Lundstroem, I. *J. Colloid Interface Sci.* **1991**, *147*, 103.
42. Fadeev, A. Y.; McCarthy, T. J. *Langmuir* **2000**, *16*, 7268.
43. Tseng, Y.-C.; Phoa, K.; Carlton, D.; Bokor, J. Effect of Diameter Variation in a Large Set of Carbon Nanotube Transistors. *Nano Lett.* **2006**, *6*, 1364–1368.
44. Kang, S. J.; Kocabas, C.; Ozel, T.; Shim, M.; Pimparkar, N.; Alam, M. A.; Rotkin, S. V.; Rogers, J. A. High-Performance Electronics Using Dense, Perfectly Aligned Arrays of Single-Walled Carbon Nanotubes. *Nat. Nanotechnol.* **2007**, *2*, 230–236.
45. Gruner, G. Carbon Nanotube Films for Transparent and Plastic Electronics. *J. Mater. Chem.* **2006**, *16*, 3533–3539.
46. Jorio, A.; Saito, R.; Hafner, J. H.; Lieber, C. M.; Hunter, M.; McClure, T.; Dresselhaus, G.; Dresselhaus, M. S. *Phys. Rev. Lett.* **2001**, *86*, 1118.
47. Dresselhaus, M. S.; Dresselhaus, G.; Jorio, A.; Souza Filho, A. G.; Saito, R. Raman Spectroscopy on Isolated Single Wall Carbon Nanotubes. *Carbon* **2002**, *40*, 2043–2061.